Geoderma 464 (2025) 117611

Contents lists available at ScienceDirect

Geoderma

journal homepage: www.elsevier.com/locate/geoderma

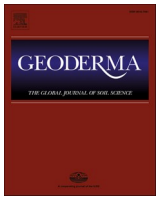

Short-term impact of mechanical loosening on physical soil properties in a severely compacted subsoil

Alina Widmer [a], Alice Johannes [a], Mario Fontana [b], Marlies Sommer [a], Saïd Elfouki [b], Luca Bragazza [b], John Koestel [a,*]

[a] Agroscope, Soil Quality and Soil Use, Reckenholzstrasse 191, 8046 Zurich, Switzerland
[b] Agroscope, Field-Crop Systems and Plant Nutrition, Route de Duillier 60, 1260 Nyon, Switzerland

ARTICLE INFO

Handling Editor: Yvan Capowiez

Keywords:
Subsoil
Compaction
Subsoil compaction
X-ray imaging
Mechanical soil loosening
Soil structure
Soil physics
Air permeability
Air diffusion
Water retention
Penetration resistance
Connectivity

ABSTRACT

Subsoil compaction is a serious threat to the fertility of our urban and agricultural lands. In severe cases it impedes aeration of and water infiltration into the subsoil, increasing risks of water-logging and overland run-off with erosion. It also may prevent roots from growing to larger depths, being unable to exploit subsoil water resources in the case of droughts. In this study we investigated soil structural properties in the aftermath of a heavy compaction event caused by storage of excavated soil in an approximately 10 m tall heap over several years. In addition, we evaluated mechanical loosening with a digger to ameliorate the subsoil physical properties. We contrasted soil physical properties of undisturbed soil samples (100 cm^3 volume, sampled approximately 9 months after the subsoil loosening) as well as X-ray image-data of compacted, mechanically loosened and pristine subsoil down to approximately 80 cm below the soil surface. We found that the soil loosening improved penetration resistances, porosities and soil aeration properties, especially in the deepest investigated soil layer at 60 cm depth. At this depth, the loosened soil had similar or even better properties than the pristine soil. The compacted soil was almost completely devoid of X-ray imaged macropores. In contrast, the loosened soil featured similar imaged porosities as the pristine soil, but was lacking biopore networks, which resulted in a less well-connected imaged pore system and decreased soil aeration under wet conditions. Note that classical pore-network connectivity measures like the Gamma connectivity or the Euler number turned out to be unsuited as indicators of severely degraded pore networks like in our study. Instead, we encourage the use of approaches from percolation theory to quantify loss of macropore connectivity in compacted soil, for example the critical pore diameter or the number of samples with an imaged connection from top to bottom surface per treatment. Our results demonstrate the beneficial effects of mechanical soil loosening of severely compacted subsoil to soil macropore-networks and associated soil functions. However, our results also confirm that natural and mechanically-loosened soil structures are clearly dissimilar. Time is required until the loosened subsoil has consolidated and re-developed a biopore network, albeit the loosening is expected to shorten the time for subsoil recovery considerably. Future studies are necessary to evaluate the persistence of effects of comprehensive soil loosening of heavily compacted subsoil.

1. Introduction

Soil structure is defined as the spatial arrangement of pores and solids in soil (Rabot et al., 2018). A good soil structure provides functions that deliver vital ecosystem services, such as exchange of gases like oxygen and CO_2 with the atmosphere, transport and purification of water, storage of water and nutrients, paths of least resistance for root growth and habitats for edaphic organisms. Ideally, soil structure is characterized by a well-connected and stable pore-network (Dexter, 1988) and a soil matrix that is loose enough to allow roots to grow (Bengough et al., 2011).

The use of heavy machines and construction of buildings and infrastructure has become more frequent in the recent years, which increases the threat of soil compaction (Berli et al., 2004). Soil compaction deteriorates soil structural properties by reducing soil porosity and pore connectivity. The macropores are most severely affected (Lipiec and

* Corresponding author.
E-mail address: Johannes.koestel@agroscope.admin.ch (J. Koestel).

https://doi.org/10.1016/j.geoderma.2025.117611
Received 14 July 2025; Received in revised form 14 October 2025; Accepted 16 November 2025
Available online 25 November 2025

Hatano, 2003). Gas, water and nutrient flows are partly inhibited (Keller et al., 2021; Schäffer et al., 2007), ecological niches in the soil shift to more anaerobic conditions (Berisso et al., 2012; Drew, 1992), the soil loses water storage potential (Keller et al., 2019) and becomes more susceptible to preferential flow or even surface runoff (Mossadeghi-Björklund et al., 2016). Soil compaction also leads to increased soil penetration resistances and may become too dense for roots to penetrate (Gao et al., 2016). Since soil compaction affects physical, biological, and chemical soil properties, the sum of all these effects can lead to significant soil degradation (Batey, 2009).

Detailed investigations on 3-D soil structures have been mostly focused on the topsoil as soil samples are easier to retrieve close to the soil surface. It is important to extend such research also to the subsoil (at depths of more than 20–30 cm) where a good soil structure is also important. As subsoils hydraulically connect topsoil with the groundwater, subsoil compaction may cause water-logging in the topsoil, thus inhibiting seedling emergence and crop growth (Colombi et al., 2018). At the same time, gas exchange of subsoil air with the atmosphere is compromised, decreasing soil fertility. Under severe subsoil compaction roots cannot penetrate to grow to deeper soil volumes. This is undesirable, as subsoils greatly increase the reservoir of available water that plants can access under droughts (Kautz et al., 2013). In this case, carbon input into the subsoil by root growth would be reduced. In this fashion carbon sequestration potential in deeper soil layers may remain unused, as subsoils also serve as an important storage of organic carbon (Meurer et al., 2018; Rumpel et al., 2012).

Subsoil compaction may not be readily discovered since it is hidden below the topsoil and it only manifests in indirectly observable effects. Recovery of subsoil structure takes longer than the topsoil, because soil structure forming processes occur less frequently or lose power with increasing depth (Håkansson and Reeder, 1994). Bioturbation and biological activity in the subsoil are reduced due to scarcer food resources, oxygen supply and increased soil strength. Wetting-drying cycles have smaller amplitudes (Schjønning et al., 2015). Additionally, if penetration resistance is too high, root growth is limited thereby reducing the formation of biopores (Cresswell and Kirkegaard, 1995) and further decreasing the activity of the soil fauna. Consequently, it has been observed that natural subsoil recovery usually takes more than a decade (Berisso et al., 2012; Peng and Horn, 2008) and has been estimated to possibly require centuries (Etana et al., 2013; Schjønning et al., 2015). It has even been argued that subsoil compaction may be permanent without external aid (Håkansson and Reeder, 1994).

Literature on subsoil remediation after compaction is still relatively scarce (Berisso et al., 2012; Keller et al., 2017). Besides bio-subsoiling (cropping of deep-rooting plants, e.g. Pulido-Moncada et al., 2020), mechanical loosening has been proposed as an external aid to speed up the remediation. The goal of mechanical loosening is to support the natural recovery mechanisms that strengthen soil resistance against compaction (Spoor, 2006). Soil resistance increases due to enmeshment by fungal hyphae and roots and the development of biopore-networks. The latter are known to be less susceptible to soil compaction than abiotically created cracks and fissures (Schäffer et al., 2008a; Schäffer et al., 2008b). A loosened soil offers better aeration and water infiltration, which create more abundant and more attractive habitats for soil fauna. At the same time, the soil is easier to penetrate, which promotes root growth and burrowing activities of soil fauna (Hamza and Anderson, 2005). Subsoil is loosened with different techniques depending on the degree of compaction and equipment available (Sinnett et al., 2006). In agriculture, the soil is often subsoiled by ripping the soil without turning the soil horizons (Schneider et al., 2017). If the compaction exceeds a certain limit, subsoiling is not possible due to the high mechanical resistance of the subsoil. In this case, a digger is used that lifts and drops the soil material in the hope that the dropped soil volume shatters and loosens on impact (Sinnett et al., 2006). The long-term success of mechanical loosening depends strongly on the aftertreatment of the soil. It is advised to omit heavy traffic on a recently ameliorated soil, especially at moist conditions, since the soil is prone to re-compaction until a more stable soil structure with biopore networks has developed (Munkholm et al., 2005; Schäffer et al., 2007).

During the recent years, non-invasive imaging techniques like X-ray imaging offer additional means to investigate the impact of soil compaction and subsequent loosening intervention. Pioneering work taking advantage of three-dimensional (3-D) X-ray imaging in this field of research was conducted in the studies of Kremer et al., (2002) and Schäffer et al., (2007). Since then, additional, similar studies have been published (Kim et al., 2010; Lamandé et al., 2013; Tian et al., 2023). However, only a few of these studies, like (Pöhlitz et al., 2019) take full advantage of the potential of 3-D X-ray imaging and quantify morphological pore network features. Meanwhile it is also possible to quantify the fraction of biopores in X-ray image data, which has potential to act as means to appraise the state of soil structural recovery. We are not aware of any study quantifying the short-term impact of soil loosening operations on the macropore network.

In this study, we investigated the impact of a severe subsoil compaction as well as the short-term efficiency of mechanical loosening on the macro-pore network structure, the pore-size distribution of larger pores and associated physical properties like penetration resistance, air permeability and oxygen diffusion. We contrasted the results from the compacted and loosened plots with the ones from a neighbouring uncompacted reference plot. We hypothesized that the mechanical loosening led to soil structural properties associated with significantly enhanced soil functions. At the same time, we expected the loosened soil structure to be of inferior quality compared to the one of the reference soil due to less connected macropores due to a lower number biopores.

2. Site description

2.1. Study site and soil properties

The study site is part of the research domain of Agroscope – Nyon (Switzerland, 46°23′53.1″ North and 6°13′43.4″ East, 447 m above sea level). According to World Reference Base taxonomy (IUSS, 2022), the soil is classified as a"Pseudogley calcaire" (corresponding to a Calcaric Stagnosol in the World Reference Base soil classification; IUSS, 2022) with a depth of 71–100 cm (Bonard, 1982). The soil has a loamy texture (Table 1). Brick fragments were found while sampling part of the investigated area so that the abundance of brick fragments raises the question of whether classifying the soil of this part of the study site as an anthroposol would be more accurate.

2.2. Soil compaction

During the construction works of a new building nearby, the study site was used as a deposit area for excavation material from 2013 to July 2019 (Fig. 1a and b). Prior to the construction works, the topmost 25 cm of the soil at the deposit area had been removed as a soil protection measure. The excavation material was then piled directly onto the subsoil. During the years, the deposit reached heights of more than ten

Table 1
Soil properties at the study site.

Depth (cm)	Plots	Clay (g g^{-1})	Silt (g g^{-1})	Sand (g g^{-1})	Soil organic matter (g g^{-1})
0–10	compacted/ loosened	0.25	0.43	0.32	0.017
	reference	0.29	0.42	0.29	0.016
10–20	compacted/ loosened	0.25	0.44	0.31	0.014
	reference	0.29	0.44	0.28	0.014
20–50	compacted/ loosened	0.26	0.44	0.3	0.01
	reference	0.3	0.44	0.26	0.011

Fig. 1. (a) The pile of excavation material seen from the side. Note the van and the two persons at the right of the image for scale; (b) the pile of excavation material seen from above in spring 2015; (c) mechanical subsoil loosening with a digger in June 2020.

meters (Fig. 1a). The long-standing overlying pressure of the excavation material resulted in a high degree of subsoil compaction. After the construction work was finished, the excavation materials were removed and the original topsoil was put back on the now compacted subsoil. In July 2019, compost was added on the subsoil compacted area. Then, a subsoiling to 50 cm depth was attempted but was given up after it became obvious that the degree of compaction was too large to penetrate the subsoil. A cultivator was used to level the partially ripped open soil and destroy weeds. Then a rotative harrow was applied for seedbed preparation and alfalfa (*Medicago sativa*) was seeded and the soil was rolled. Shortly thereafter, an investigation by the cantonal soil protection authority for construction sites ("Bodenkundliche Baubegleitung") enforced that the subsoil was to be loosened with help of a digger. It was then decided to use the study site to investigate the efficiency of the soil loosening approach for speeding up subsoil recovery.

On 7th to 8th July 2020, half of the compacted area was loosened mechanically. The uncompacted topsoil was removed once more and a digger was used to excavate the subsoil to a depth of 80 cm, lift the soil material and drop it from a height of 200 cm to break it down into smaller clods (Fig. 1c). Only half of the area of the compacted site was loosened mechanically, and the remaining area was left compacted and unchanged (Fig. 2b). After re-applying the topsoil on the loosened subsoil, the whole compacted area as well as a neighbouring reference plot (Fig. 2b) that served as a reference were ploughed to a depth of 20 cm. Then, seedbeds were prepared and a grass-legume mixture (UFA gold 320, containing alfalfa and rye grass, among others) was sown whereupon the soil was rolled and watered. Care was taken to avoid re-compaction of the areas with loosened subsoil during these soil management operations. Table 2 gives an overview on the field operations at the site shortly prior, during and after the soil compaction.

2.3. Soil sampling

Since the level of soil compaction was heterogeneously distributed over the investigated area, we decided to take samples from a subsection where the penetrometer resistance prior to the loosening was at a comparable level for compacted and loosened treatments. Here, we chose each three adjacent blocks per treatment with dimensions of 8.3 by 10 m^2 as depicted in Fig. 2b. The sown grassland had well established at the study site when the soil samples were taken on 19th and 20th April 2021. Differences in plant species dominance in relation to the treatment were clearly visible, with alfalfa dominating on the compacted parts and rye grass on the loosened parts. We acquired undisturbed soil samples by first manually drilling bore-holes down to the sampling depth using Riverside augers (Eijkelkamp) and to remove the overlying soil. We then obtained the samples by gently hammering in retrieving aluminium rings using Eijkelkamp sample holders with bayonet connection with appropriate length extensions for the subsoil. The aluminium rings were approximately 5.1 cm tall with an inner diameter of 5 cm and a volume of 100 cm^3. Due to an unusually dry spring, the topsoil was relatively dry with a matrix potential of −870 hPa measured at a nearby field site (located within 1 km distance). At 60 cm depth, the soil at this station was approximately at field capacity (−96 hPa), reflecting moister conditions that were also visually observed during sampling. Soil samples were taken from 10 cm (7.5 to 12.5 cm, topsoil), 30 cm (27.5 to 32.5 cm, upper subsoil), and 60 cm (57.5 to 62.5 cm, lower subsoil) depth in the compacted, loosened, and reference treatment (Fig. 2b). A total of 135 samples were taken, 15 at each depth and treatment (five sampling positions per block). Due to the dry conditions, three of the 45 topsoil samples were of overly poor quality and discarded. Therefore, the analysis of the undisturbed soil cores was conducted on 132 samples.

2.4. Penetration resistance

A first penetration resistance measurement campaign in 2020 was undertaken on 22th January 2020. By then, the soil loosening had not yet been carried out. Three days before the measurement, a precipitation event of approximately 10 mm that had occurred at the site. The matric potential measured at the nearby field station was −25 hPa at 30 cm and −51 hPa at 60 cm depth, suggesting a soil wetness above field capacity during the measurement. The instrument used was an Eijkelkamp Penetro Viewer Vs. 6.08 with a cone area of 1 cm^2 and a cone-angle of 60°. The depth resolution of the soil resistance was 1 cm. Measurement were taken in a 5 by 5-meter grid over an area of 60 × 50 m^2, respectively, covering the extent of the former pile of excavation material and the area on which the removed topsoil had been deposited. A map of the

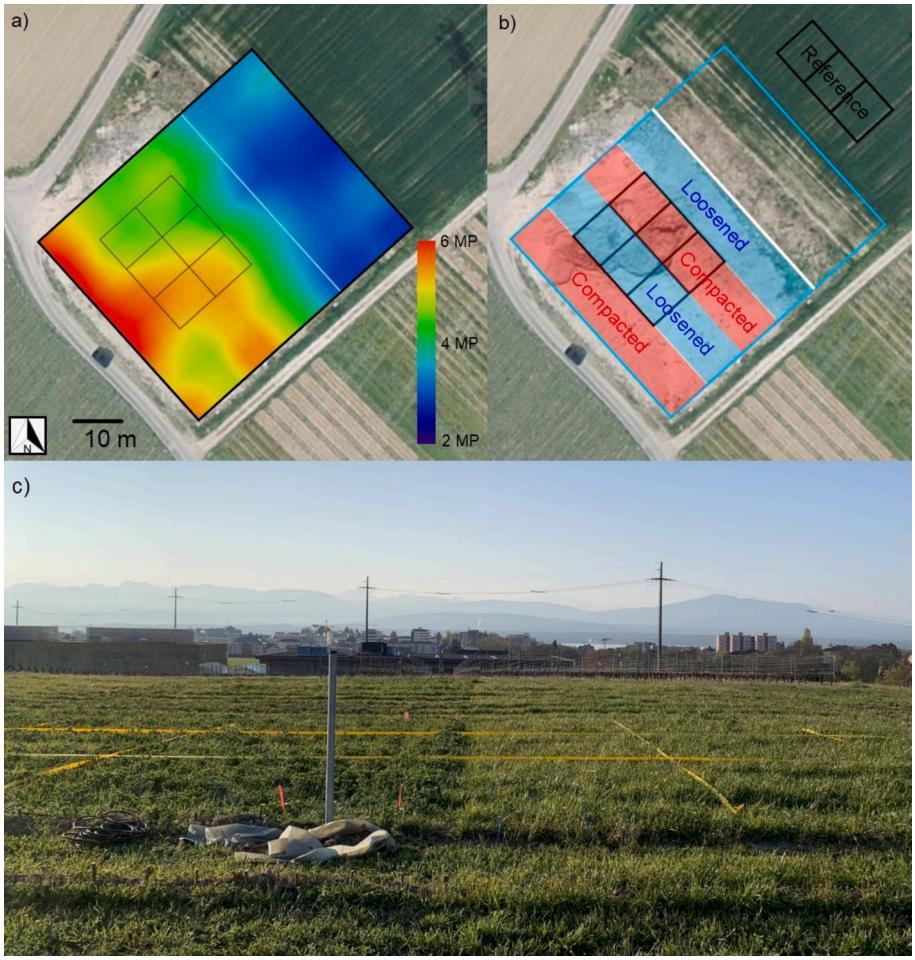

Fig. 2. (a) Aerial view of the study site with a map of the penetration resistance at 50 cm soil depth measured in January 2020, prior to the soil loosening operation. A Gaussian blur filter was applied to the penetrometer data to improve discernability of patterns. The black outlines delineate the sampling plots for the compacted and loosened treatment. (b) Aerial view on the study site depicting the sampling areas according to treatments (compare to Fig. 1b). The blue bounding box delineates the area on which the penetrometer measurements were conducted. The black outlines delineate the positions of the sampled plots for compacted, loosened and reference treatments. (c) View along the boundary between the sampled loosened (right) and compacted (left) treatments towards the south-east just before soil sampling. The loosened plots were dominated by rye grass, the compacted plots by alfalfa.

penetration resistance at 50 cm depth is given in Fig. 2a. For statistical analyses, we interpolated four penetration resistance profiles per block and treatment, using a distance-based weighing scheme. For each investigated depth range, the median value of all included depth was taken. In addition, 12 penetration resistance profiles were measured on the reference plots, which were located outside the mapped area, as shown in Fig. 2b.

The penetration resistance was measured a second time on the 4th of November 2021, approximately 15 months after the soil loosening. More than 50 mm of rainfall had been registered during the five days prior to the measurement. The matrix potential at the nearby field was −13 hPa (30 cm depth) and −10 hPa (60 cm depth), respectively. Instead of a penetrologger, an Eijkelkamp hand penetrometer Vs. 6.01 was used. The cone area was again 1 cm^2 the cone-angle of 60°. The depth resolution of penetration resistance was 5 cm. Four replicated penetration resistance profiles were measured per block. Measurements were carried out to a depth of 60 cm.

2.5. Water retention curves

We measured water retention curves for the intact 132 undisturbed soil samples using pressure steps of −30, –100 and −300 hPa. The soil samples were saturated slowly from the bottom with degassed tap water. They then were placed on suction plates (EcoTech). We estimated the amount of large ($ø > 100$ μm) and small ($100 \geq ø > 30$ μm) macropores as well as large mesopores ($30 \geq ø > 10$ μm) from the water retention curve assuming the suitability of Young-Laplace's law and fully wettable soil.

2.6. Oxygen diffusion and air permeability

Oxygen diffusion and air permeability were measured on the 132 samples after they had been equilibrated to −30, −100 and −300 hPa. We determined the oxygen diffusivity using the chamber method detailed in Martinez et al., (2016). The soil samples were connected with the top surface to a small chamber, so that gas exchange between chamber and the outside was only possible through the soil sample. Then the air in the chamber was replaced by N_2 gas and the rate of increase in oxygen was measured that diffused back through the soil into the chamber. From the rate of oxygen increase, the relative oxygen diffusion coefficient D_p/D_0 (a.k.a. diffusivity, unitless) was calculated as explained in Schjønning et al., (2013). Here, D_p ($cm^2\ h^{-1}$) is the oxygen diffusion coefficient in the soil and D_0 ($cm^2\ h^{-1}$) is the one in free air. Influences of temperature and atmospheric pressure on the measurements were corrected following (Martinez et al., 2016).

We used a steady-state airflow setup to quantify the air permeability as described in Martinez et al., (2016). The soil columns were mounted to a lid through which air was conducted. The lid was placed tightly on

Table 2
Summary of cropping, soil management and fertilization history of the study site from 2009 to 2020.

Year	Plot	Crop establishment	Subsoiling (50 cm)	Tillage (20 cm)	Rotary	Rototiller	Compost	N (kg ha^{-1})	P_2O_5 (kg ha^{-1})	K_2O (kg ha^{-1})	MgO (kg ha^{-1})	CaO (kg ha^{-1})
2009	All	Spring wheat (03/23)	–	(12/15)	(03/23)	–	–	110.2	–	–	–	–
2010	All	Spring Oat (04/20) Green manure	–	(04/20) (11/22)	(04/20)	–	–	89.8	–	257.4	–	–
2011	All	Sunflower (04/07)	–	–	(04/07)	–	–	50.8	–	–	72	–
2012	Pile	Winter wheat (10/12/2011)	–	–	–	–	–		–	–	–	–
	Reference		–	–	(07/25)	–	–		–	–	–	–
2013	Pile	Pile	Pile	Pile	Pile	Pile	Pile	Pile	Pile	Pile	Pile	Pile
	Reference	Spring barley (04/17) Rapeseed (08/30)	(13/08)	(04/09)	(04/17) (08/29)	–	–	139.7	–	–	32	–
2014	Pile	Pile	Pile	Pile	Pile	Pile	Pile	Pile	Pile	Pile	Pile	Pile
	Reference	Winter wheat (10/13)	–	–	–	–	–	–	–	–	–	–
2015	Pile	Pile	Pile	Pile	Pile	Pile	Pile	Pile	Pile	Pile	Pile	Pile
	Reference	Green manure (07/25)	–	(11/19)	(08/20)	(10/02)	0	149.3	0	0	20.3	
2016	Pile	Pile	Pile	Pile	Pile	Pile	Pile	Pile	Pile	Pile	Pile	Pile
	Reference	Maize (05/09)		(11/02)			0	119.6	209.8	314.7	5.5	
2017	Pile	Pile	Pile	Pile	Pile	Pile	Pile	Pile	Pile	Pile	Pile	Pile
	Reference	Soybean (05/17)		(10/25)	(05/17)	(02/27)	110 (N unit) (02/20) = 87.6 m^3	11	330	550	330	356
2018	Pile	Pile	Pile	Pile	Pile	Pile	Pile	Pile	Pile	Pile	Pile	Pile
	Reference	Spring Wheat (03/23)		(03/23)				113			17	9
2019	Pile	Alfalfa (08/19)	Attempted (07/03)	–	–	(07/03)	93.777 (N unit) (07/02) = 30 m^3	–	281	469	281	303
	Reference		–			–	–					
2020	Pile	Grassland UFA 321 gold (08/19)	decompaction with digger (07/07)	–	(08/05)	(08/25)	–	–	–	–	–	–
	Reference	Grassland UFA 321 gold (08/25)	–									

the aluminium rings holding the soil samples so that the entire airflow was forced through the soil sample. We adjusted a small pressure gradient of 2 hPa for which laminar flow can be assumed. Then the flow rate was determined and calculated to an air permeability using Darcy's equation, taking temperature effects on the air viscosity into account.

2.7. X-ray tomography

2.7.1. Image acquisition

Soil samples were scanned at the ETH in Zurich with an X-ray scanner GE phoenix v|tome|x s 240 featuring a GE DXR250 HCD (4MP) detector plate with 2024 × 2024 crystals in x and y directions (GE Sensing Inspection Technologies GmbH, Wunstorf, Germany). At the time of the X-ray measurements, all soil samples were at a matrix potential of −100 cm. To limit image noise and shorten the image acquisition time, a two-by-two binning was used. We applied 0.7 mm of copper as an optical filter to remove photons of low energies from the beam and thus reduce potential beam hardening artefacts. The X-ray tube was operated with an electron flow of 420 µA with a voltage of 150 kV. The voxel resolution was 63.2 µm. We assume in the following that respective image resolution was approximately twice the voxel size (126 µm). We therefore denote all imaged pores as large macropores, being aware that the image resolution was somewhat worse than the pore-size threshold defining large macropores for the water retention curve data. 2098 radiographs from individual angles were collected per 3-D image. The total scanning time per sample was 7 min. A 16-bit unsigned grayscale was chosen for the image reconstruction to keep the file size within reasonable limits (2 GB). Twenty-six samples were scanned in October 2021. Then, the X-ray scanner broke down and was not operational until February the following year. The remaining 106 samples were scanned five months later, in February 2022 when the scanner was operational again. During the five months, the samples were stored in a room at 4 °C to limit bioactivity and covered with lids on both sides to minimize water evaporation.

2.7.2. Image evaluation

For image processing, the ImageJ/FIJI software was used (Schindelin et al., 2012). If not stated otherwise, the following steps were conducted using the plugin SoilJ version 1.2.18 for image processing (Koestel, 2018), which also incorporates several functions of MorphoLibJ (Legland et al., 2016). First, the 3-D images were straightened and centred on the 3-D canvas and the wall coordinates, top and bottom of the column, were identified with SoilJ. A 3D adaptive Gaussian filter was applied with a 2 × 2 × 2 kernel size to remove noise from the image (Ollion et al., 2013). We calibrated all images to a common grey-scale using air-filled pores and the aluminium wall as reference values. Here, we applied the following correction function to each horizontal image layer:

$$v_{i,c} = \frac{(v_i - v_{air})}{(v_{alu} - v_{air})}(t_{alu} - t_{air}) + t_{air} \quad (1)$$

where $v_{i,c}$ is the corrected grey-value value of the voxel at position i, v_i, v_{air} and v_{alu} are the uncorrected grey values at position i as well as of the air and the aluminium in the horizontal layer of position i and t_{alu} and t_{air} are target values set to 20,000 and 5,000, respectively. In a first

attempt, the 0.1 percentile of the grey-values in each horizontal layer was chosen as v_{air}. However, as imaged air-filled pores ($ø > 126$ μm) were rare in the compacted soil samples, this approach did not always lead to reasonable results. For these samples, we manually selected 6 grey-values of air-filled pores from three different horizontal layers and used their median as v_{air}. This yielded a sufficiently good grey-scale calibration to proceed with the image analyses. Next, we extracted the histograms of all 132 3-D images. To each histogram, we applied a 1-D median filter with a footprint of 10 to remove noise. Subsequently, we averaged the 132 histograms to one joint histogram. We identified a grey-value of 8,000 upon visual inspection of the joint histogram and the calibrated greyscale images as an appropriate threshold to segment the air phase from all images.

Moreover, we extracted cylindrical organic objects form the 3-D images, corresponding to roots and, occasionally, earthworms. In a first step, we segmented the grey-value range between 8,000 and 12,000 corresponding to organic material. In a second step, we followed the Rootine v2 approach published by Phalempin et al, (2021). The respective algorithm is implemented into the SoilJ plugin (version 1.3.25 or higher).

All subsequent image analyses were conducted on central cylinders with a diameter of 4.3 cm, which amounts to cutting away the volumes with less than 0.38 cm distance to the aluminium walls. In this fashion, we reduced impacts from obvious sampling artefacts located predominantly close to the walls. We also discarded the top and bottommost 0.44 cm of each 3-D image to exclude Feldkamp imaging artefacts, that typically manifest at the top and the bottom of X-ray imaged object for cone-beam scanners with vertically fixed rotating manipulators (see e.g. Kudo and Saito, 1994).

We quantified the grey-values of the soil matrix as an indicator for its density. This is a valid approach as the samples had been adjusted to a matrix potential of −100 hPa prior to scanning. The soil matrix grey-values were therefore not biased due to differing saturation levels between individual samples. We used SoilJ to extract morphological properties of the imaged macropore network. These were the imaged porosity, the pore size distribution of the macropores, the fraction of biopores, percolation properties of the imaged pore network as well as the Gamma connectivity and the Euler number of the pore network. The fraction of biopores was obtained following the approach outlined in Lucas et al., (2019), as implemented into SoilJ. The approach identifies a measure for how much a pore locally resembles a cylinder, assuming that cylindrical pores correspond to biopores. In percolation theory, the term 'percolation' denotes the existence of a connected path between two surfaces of a domain. In our case, percolation was true when there was an imaged pore connection from top to bottom of the sample. The critical pore diameter is the diameter of the bottleneck in the pore connection from top to bottom (Jarvis et al., 2017). The Gamma connectivity expresses the probability that two randomly chosen pore voxels are connected to each other (Renard and Allard, 2013). In our study, the Euler number is simply the difference in the number of unconnected pore-clusters and redundant connections (loops) in the imaged pore network, as cavities in the pore network are physically nonsensical.

2.8. Statistics

The data analysis was conducted with Python 3.9 and R 4.2.3. As the inhomogeneous soil compaction did not allow for a randomized block design, we treated all 15 undisturbed soil samples per treatment and depth as independent replicates. Similarly, penetration resistance measurements were considered only dependent on the treatment within which they were taken. Since the topsoil was removed prior to compaction, this soil depth was a separate model. The statistical model of the subsoil depended on depth and treatment. First, the data was checked for normal distribution using a Shapiro Wilk test. If the data was not normally distributed, they were transformed logarithmically or by taking the square root. Furthermore, the data was analysed for homoscedasticity with a Breusch-Pagan test. If the normal distribution was not reached and the variance was unequal, a Kruskal Wallis test was used. If the data was normally distributed and homoscedastic, a one-way ANOVA was carried out. To enhance the contrast and test the difference between the treatments, a post-hoc test was applied (Tukey test) and in the case of non-parametric data the Wilcoxon-test was used. We considered statistical tests with p-value of equal or less than 0.05 as significant.

3. Results

3.1. Bulk density

The bulk densities in the samples taken from 10 cm depth did not differ significantly between treatments (Fig. 3a). Bulk density tended to be larger at 30 cm depth in the compacted than for the ones from the other two treatments at 30 cm depth. In both 30 cm and 60 cm depth, mechanical loosening significantly decreased the bulk density compared to the compacted treatment. At 60 cm depth, the compacted treatment exhibited significantly the largest bulk densities observed in our study with a median bulk density of almost 1.8 g cm^{-3}.

3.2. Water retention

While the investigated porosities did not significantly differ in the topsoil, they were clearly smaller in the compacted treatment than in the other treatments at 30 cm and 60 cm depth (Fig. 3b–d). The volume of the large macropores was largest in the loosened soil in the subsoil, albeit not significantly larger than in the control treatment. Loosening significantly increased the volume of large macropores ($ø > 100$ μm) compared to the compacted treatment. The subsoil porosities for small macropore ($100 \geq ø > 30$ μm) and large mesopores ($30 \geq ø > 10$ μm) was comparable in loosened and references soil samples.

3.3. Penetration resistance

During the penetration resistance measurements in January 2020, the soil had not yet been loosened. The penetration resistance increased with depth, except for the reference plot (Fig. 4a). At depths of 30 and 60 cm, the penetration resistance in the reference plot differed significantly from the ones in the compacted area. Compacted and (not yet) loosened plots did not differ significantly (p-value: 0.18).

In the measurements conducted in November 2021 (Fig. 4b), after the loosening, the penetration resistance of the still compacted soil showed the highest and most variable penetration resistance at 30 and 60 cm depth (p-values: <0.01). The penetration resistance in the loosened plots was even significantly lower than the one in the reference plot at 30 cm depth (p-values: <0.01). The penetration resistance measured in January 2020 was significantly higher in all plots as compared to the measurements carried out in November 2021.

3.4. X-ray imaging

3.4.1. Qualitative observation

In (Fig. 5a–c, vertical cross-sections through X-ray imaged samples from different treatments are shown as examples. Fig. 5d–f shows 3-D renderings of the respective pore systems. The compacted sample exhibited only very few imaged pores (Fig. 5a and d). The loosened soil featured the macropores with the largest diameters (Fig. 5b & e). They can be described as pores in between soil fraggregates, i.e. soil aggregations created by fragmentation due to soil mechanical interventions like tillage or soil loosening (Garland et al., 2024). The soil from the reference plot featured a multitude of biopores of different diameters (Fig. 5c and f).

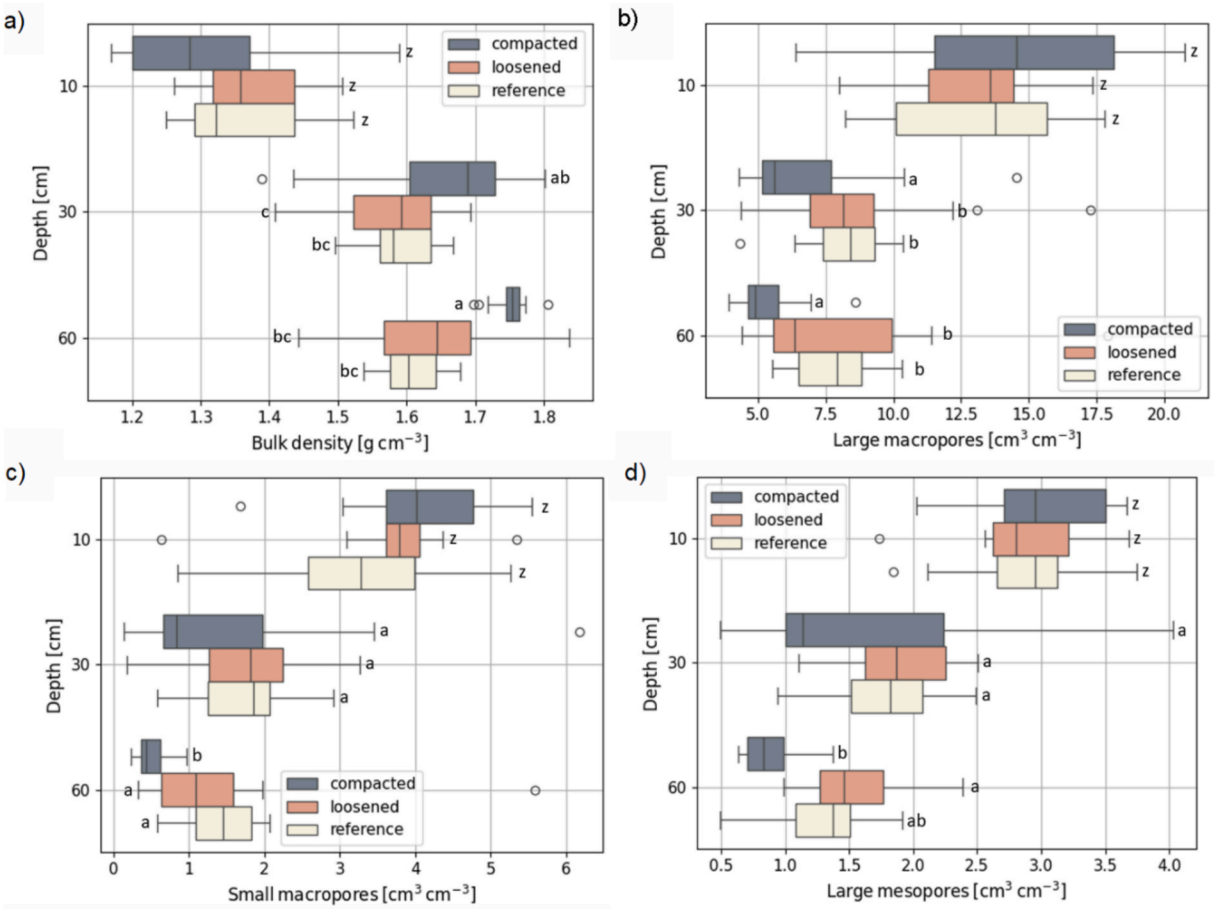

Fig. 3. (a) Bulk density and water-retention-derived volume-fractions of (b) large ($ø > 100$ μm) and (c) small macropores ($100 \geq ø > 30$ μm) as well as (d) volume fraction of large mesopores ($30 \geq ø > 10$ μm) at three depths in the three treatments. The letters indicate significantly different values for a p-value of 0.05, treating all individual soil samples per depth and treatment as independent replicates (n≈15). Note that samples from 10 cm depth were not compared to samples from 30 and 60 cm depth and, hence, different collections of letters were used.

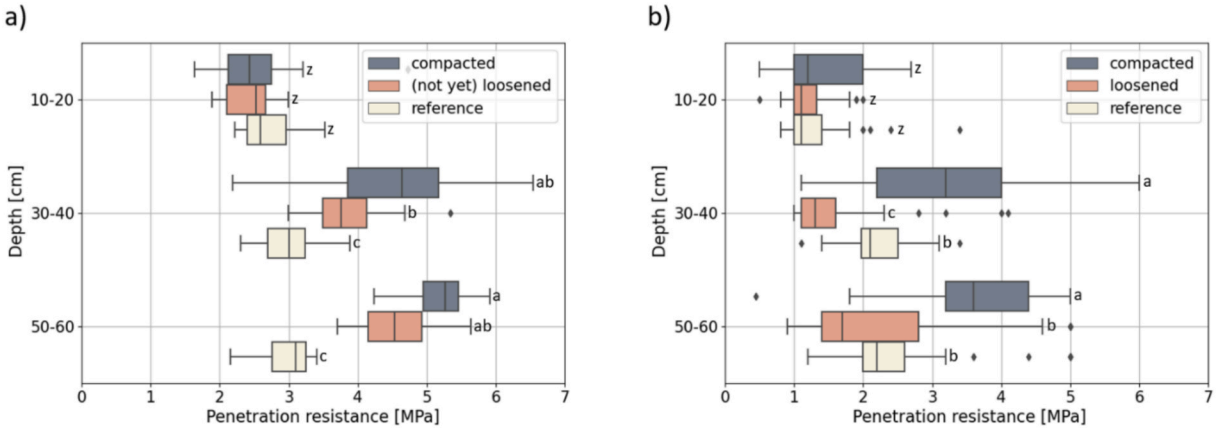

Fig. 4. (a) penetration resistances obtained in January 2020 and (b) in November 2021. The matrix potential at an adjacent measurement station was larger than −51 hPa and larger than −13 hPa across the soil profile down to 60 cm depth at the days of measurements, respectively. The letters indicate significantly different values for a p-value of 0.05, treating all individual soil samples per depth and treatment as independent replicates (n = 9). Note that samples from 10 cm depth were not compared to samples from 30 and 60 cm depth and, hence, different collections of letters were used.

3.4.2. *Histograms of the imaged soil matrix*

The histograms in Fig. 6 depict the range of grey-values corresponding to the soil matrix. With increasing sampling depth, the modes of the histograms shifted to higher grey values, indicating larger wet bulk densities of the soil matrix. Additionally, the histogram modes of the different treatments became more distinct with depth. While they were not significantly different in the topsoil (p-values: >0.12), they differed in the subsoil (p-value: <0.01). The matrix region of the histograms in the topsoil showed a larger variance as the ones in the subsoil. The variance of the soil matrix grey-values in the subsoil was largest for the loosened treatment.

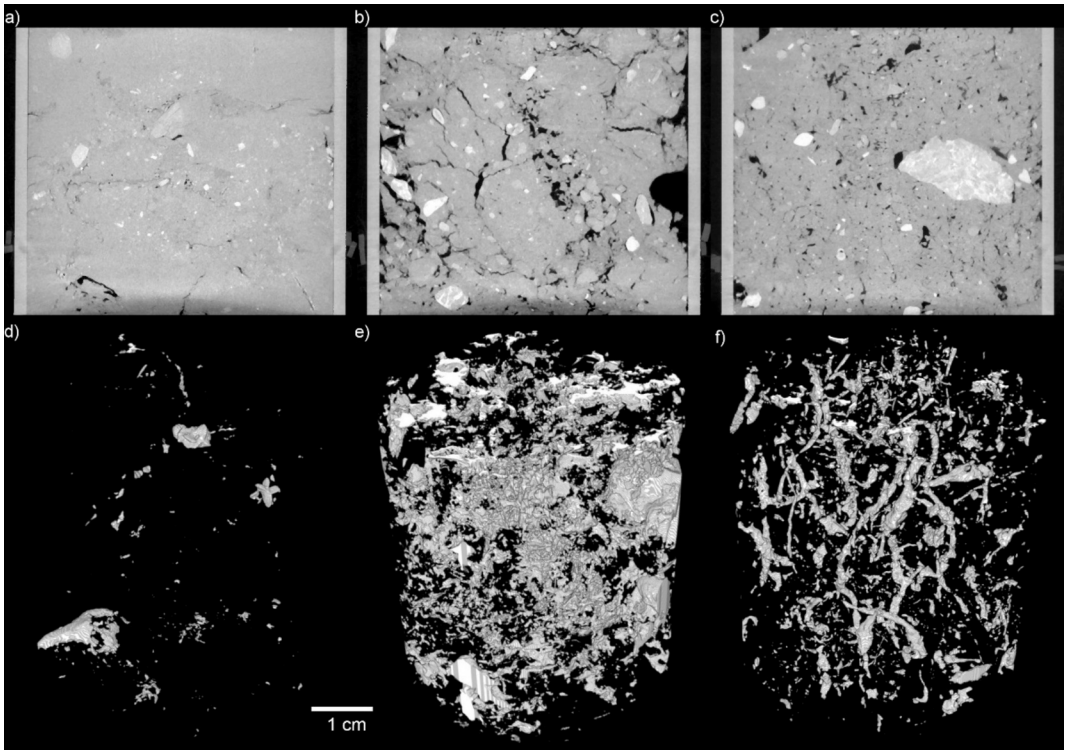

Fig. 5. Vertical cross-section through a randomly selected 3-D X-ray image of the (a) compacted, (b) loosened and (c) reference sample from sampling depths of 60 cm, respectively. The distance between the aluminum walls of the sampling rings is approximately 5 cm. In the bottom panel, the corresponding imaged macropore networks are shown from (d-f), respectively, depicting pores with diameters of more than 126 μm.

3.4.3. Imaged porosity and pore size distribution

The imaged macroporosities decreased with depth in all treatments (Fig. 7). This decrease was most drastic in the compacted treatment, which had the largest imaged macroporosities in the topsoil and the smallest in the subsoil at 60 cm depth. The opposite was found for the soil in the loosened treatments. Here, the topsoil imaged macroporosities were smallest of all treatments (only approximately half of the value found for the compacted treatment) while they were largest at 60 cm depths. At all subsoil depths, the imaged porosities in the compacted soil were significantly the smallest. At 60 cm depth, the compacted subsoil only featured a fifth of the imaged macropore volumes as the subsoil in the other two treatments. The reference soil has the widest pore diameter range in the topsoil and at 30 cm depth. At 60 cm depth, the loosened soil contained the pores with the largest diameters. Pores with diameters larger than 1.5 mm are largely missing at 30 and 60 cm depth in the compacted treatment, but also at 10 cm depth in the loosened plots.

3.4.4. Connectivity measures and percolation properties

The Gamma connectivity in the topsoil of the loosened treatment was strongly reduced as compared to the other two treatments (Fig. 8a). The respective Euler numbers (Fig. 8b) were consistent with this observation, showing a larger number of disconnected pore clusters in the topsoil of the loosened plots. In the subsoil, the reference treatment exhibited the lowest Gamma connectivities and largest Euler numbers.

Percolating imaged pore-networks were only sporadically found for the compacted and loosened subsoils, but also for the loosened topsoil. Not a single soil sample was percolating in the compacted treatment at 60 cm depths. Only in the reference subsoil, approximately half of the investigated soil samples exhibited a connection of large macropores from top to bottom (Fig. 8c). The fraction of percolating samples decreased with depth. Critical pore diameters in non-percolating soil samples must be smaller than the image resolution of 126 μm. It follows that we only found larger critical pore diameters in the reference treatment (Fig. 8d).

3.4.5. Biopores in the imaged pore-network

In Fig. 9a illustrates that the bioporosity decreased with depth in all treatments. The most biopores were found in the reference soil at all investigated depths. In the topsoil, the smallest bioporosities were detected in the loosened treatment. At larger depth, the ones identified in the compacted treatments were always the smallest.

3.4.6. Imaged roots and root-like POM

The topsoil's largest volumes of cylindrical particulate organic matter (POM,) i.e. roots and root-like POM, were found in the compacted treatment (Fig. 9b), where also its variability was largest. The reference soil showed a significantly lower content of roots and root-like POM in the topsoils as compared to both other treatments. From the topsoil to the subsoil, there was a strong decrease roots and root-like POM in all treatments. At 60 cm depth, there was nearly no roots or root-like POM in the compacted treatment.

3.4.7. Oxygen diffusion and permeability

Air diffusion increased with decreasing soil moisture and decreased with soil depth (Fig. 10a–c). No significant differences between the treatments were observed at a matrix potential of −30 hPa. At –100 hPa, the reference soil showed higher oxygen diffusion in both, 30 and 60 cm depth. At the driest investigated conditions (matrix potential of −300 hPa), the compacted treatment exhibited a smaller diffusivity compared to the value of the other treatments (p-value = 0.052). In the lower subsoil (60 cm), the air diffusion of the loosened treatment was higher than the value of the compacted treatment but did not differ significantly from the reference treatment.

Most samples in the subsoil conducted air less well than the lower bound of the measurement range of 2.3 μm^2 at a matrix potential of −30 hPa (Fig. 10d) and −100 hPa (Fig. 10e). At −300 hPa, the air permeability was lowest in the compacted subsoils, albeit not significantly

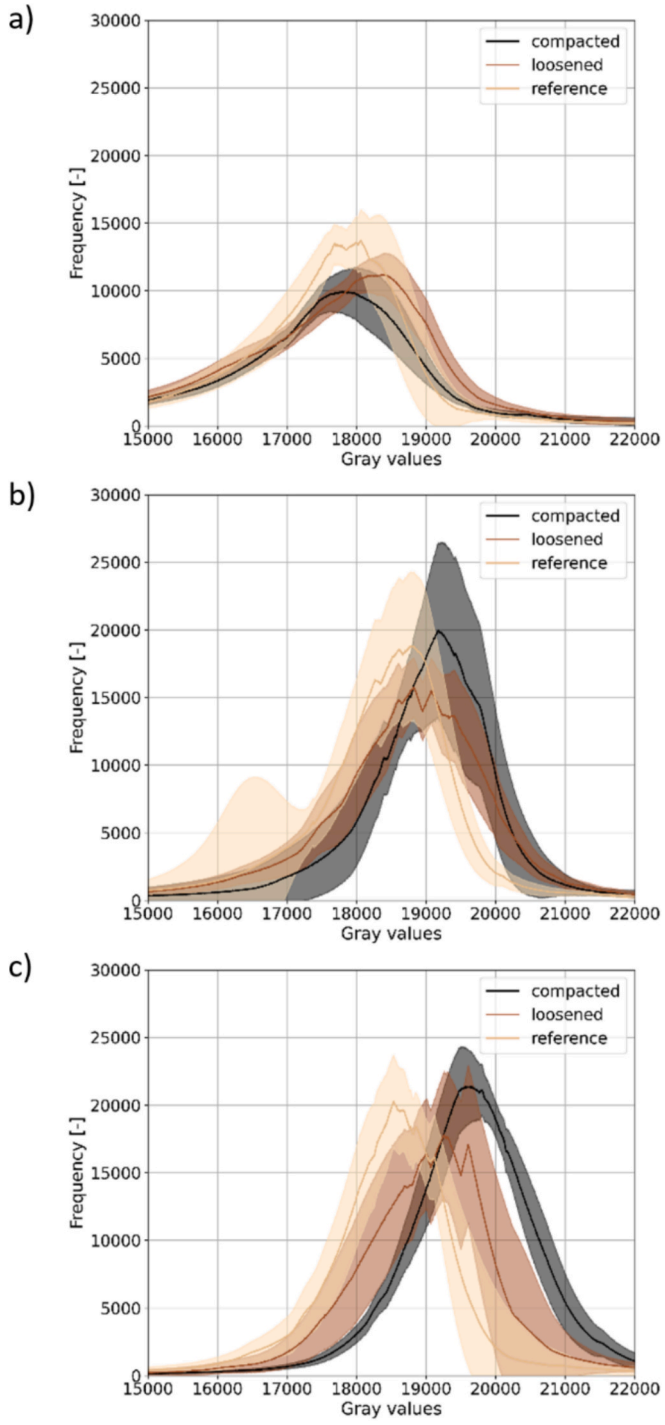

Fig. 6. The joint histogram regions corresponding to the soil matrix for all samples summarized per treatment for depths of (a) 10 cm, (b), 30 cm and (c) 60 cm. the shaded areas show the inter quartile range between the 15 replicates per depth and treatment.

(Fig. 10f). The loosened soil showed a similar air permeability as the reference soil at 30 cm depth. The air permeability in the loosened treatment was even larger than in the reference soil at 60 cm depth, however, neither significantly.

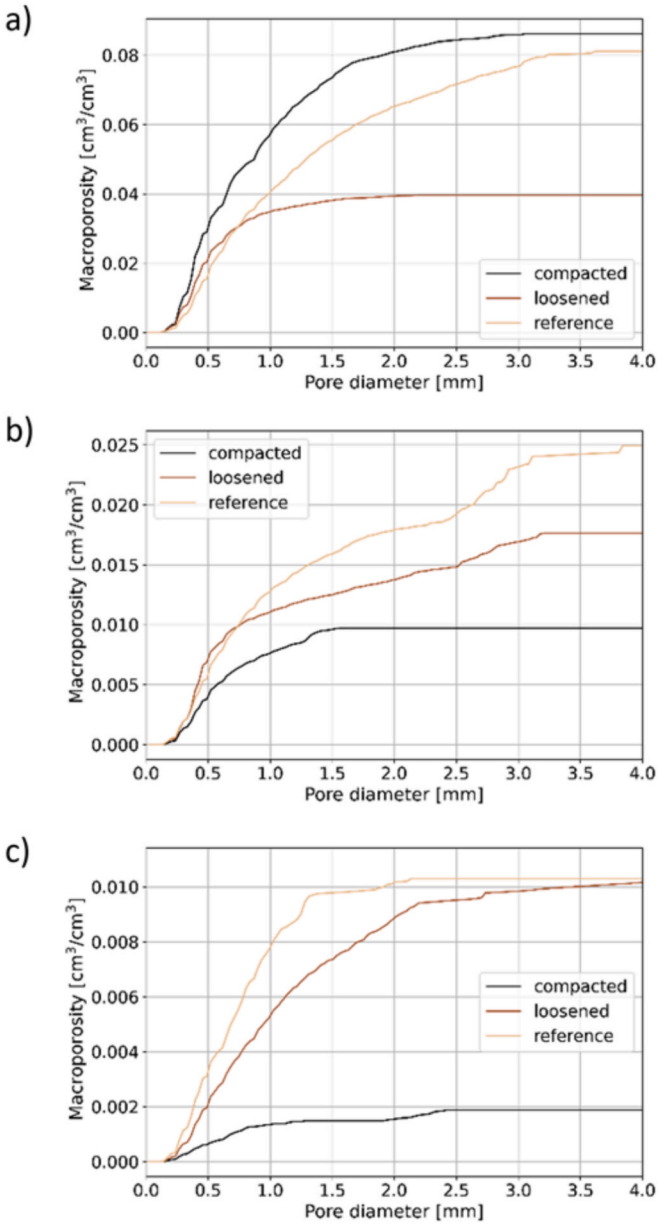

Fig. 7. Imaged macropore diameter distribution functions at (a) 10, (b) 30 and (c) 60 cm.

4. Discussion

4.1. Subsoil penetration resistance

Interpretation of penetrometer data in absolute terms is difficult, because it is strongly influenced by the soil matrix potential. Under field capacity, a threshold of 2.5 MPa has been stated as a value at which root penetration into the soil is markedly reduced (Gao et al., 2016). In our study, the penetrometer measurements were carried out under very wet conditions above field capacity, under which the penetration resistance decreases (Vaz et al., 2011). The overall reduction of penetration resistances obtained in 2021 is probably due to the larger water content in this year and the use of the different penetrometer device. Such wet conditions are not the norm during the vegetation period. We presume that the penetration resistances would have been considerably larger if we had measured at field capacity. We may therefore assume that, at field capacity, the penetration resistances of the reference soil was around or even above values of 2.5 MPa in 2021. This suggests that the

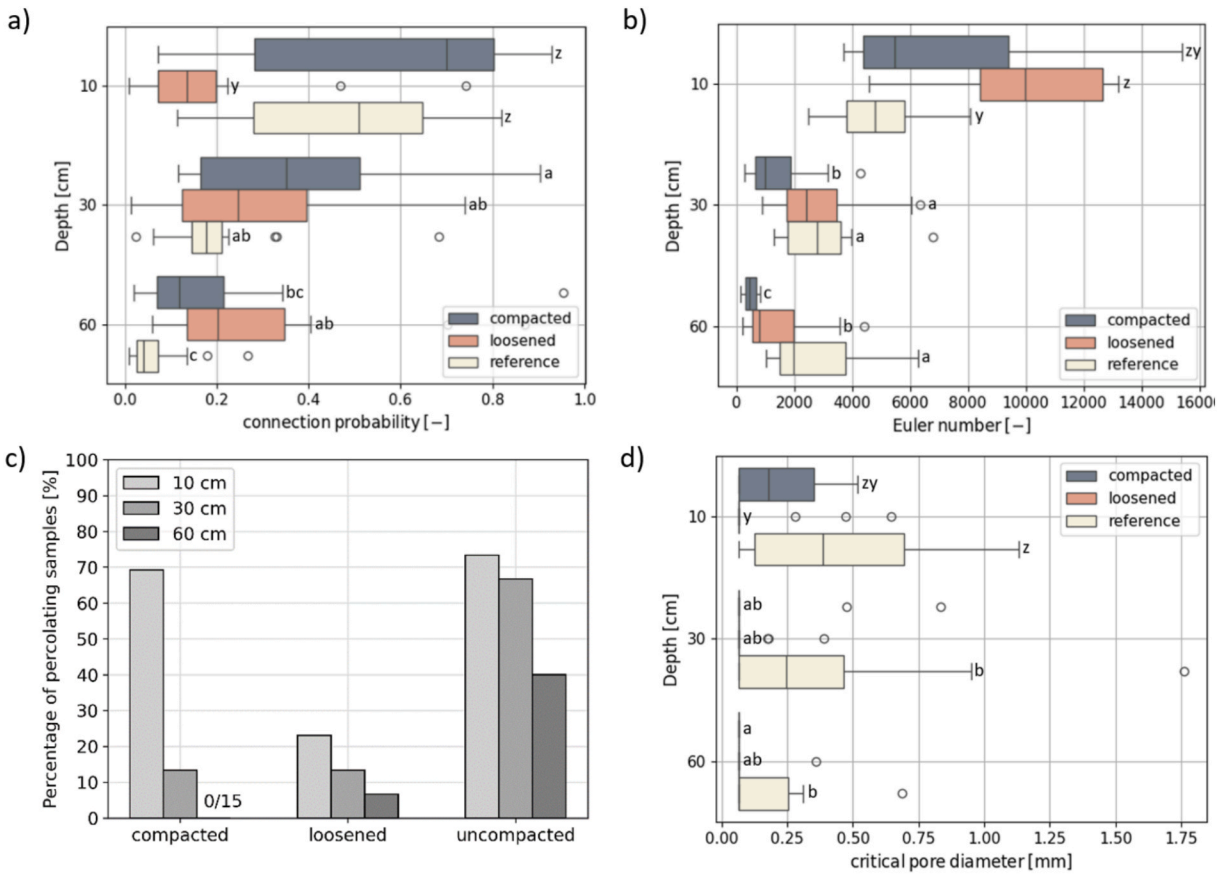

Fig. 8. (a) Gamma connectivity (a.k.a. connection probability), (b) Euler number, (c) percentage of samples with an imaged percolating pore network and (d) critical pore diameter. The letters indicate significantly different values for a p-value of 0.05, treating all individual soil samples per depth and treatment as independent replicates (n≈15). Note that samples from 10 cm depth were not compared to samples from 30 to 60 cm depth and, hence, different collections of letters were used.

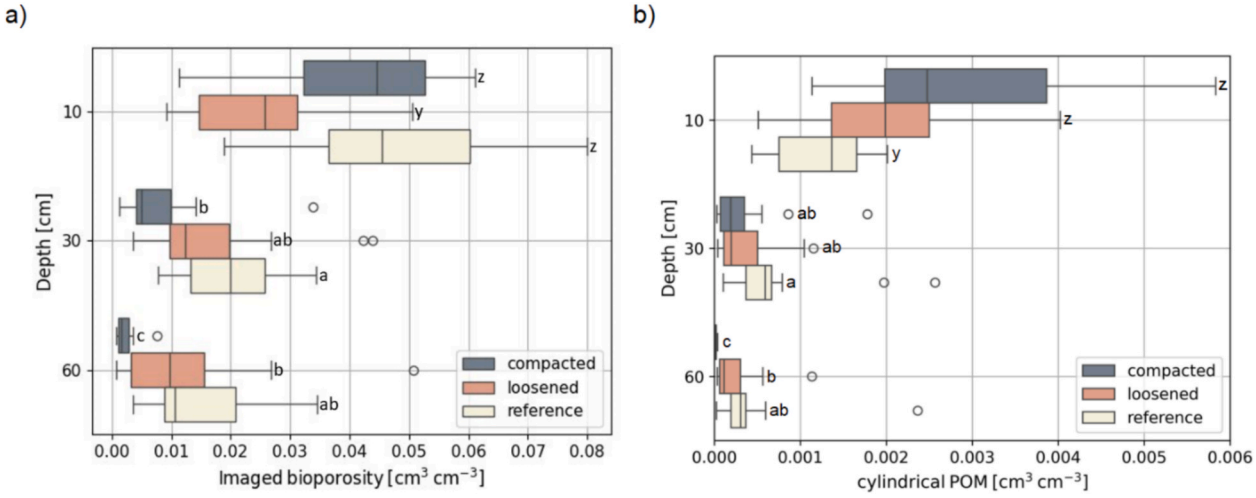

Fig. 9. (a) imaged bioporosity and (b) cylindrical particulate organic matter (POM).

reference soil also featured an elevated degree of soil compaction, rendering it suboptimal for comparisons with the compacted and loosened treatments. The X-ray images (Fig. 5) illustrate that the soil macrostructure of the loosened treatment consisted of large peds that were still compacted, but delineated by irregular cavities. This is also reflected in the somewhat larger variance of the soil matrix peak of the image histograms of the loosened treatment (Fig. 6) while the reference soil had clearly the smallest matrix density. Yet, the penetration resistances of the loosened subsoil were comparable with or lower than with the ones of the reference in 2021. This indicates a clear improvement of soil penetrability due to the soil loosening, which should be beneficial for crop growth.

4.2. *Subsoil bulk density and porosity*

The large variability of the bulk density at 30 cm depth was probably

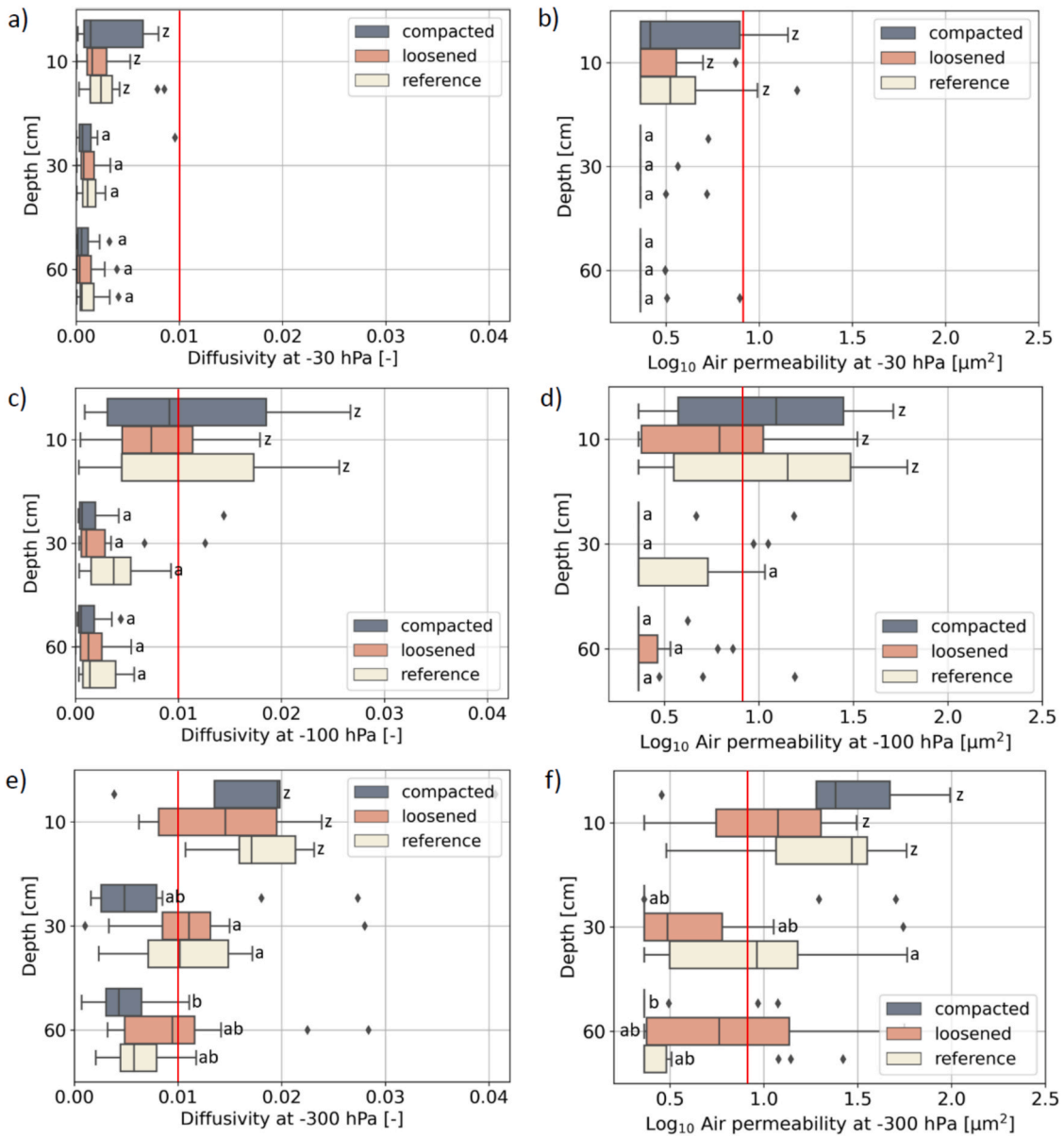

Fig. 10. (a–c) Oxygen diffusion and (d-f) air permeability at matrix potentials of (a and d) −30, (b and e) −100 and (c and f) −300 hPa. Note the log-scale for the air permeability. The red line indicates the reference values 0.01 (−) and 8.7 (μm^2) published in Horn and Hartge (2009). The letters indicate significantly different values for a p-value of 0.05, treating all individual soil samples per depth and treatment as independent replicates ($n \approx 15$). Note that samples from 10 cm depth were not compared to samples from 30 and 60 cm depth and, hence, different collections of letters were used.

caused by a varying depth of the interface between compacted subsoil and the loose topsoil, which was approximately located at this depth due to the removal of topsoil prior to the subsoil loosening. Thus, the samples were sometimes taken from the loosened topsoil and other times from the compacted subsoil. In a review, Kaufmann et al. (2010) list bulk density values for optimal root penetrability as well as threshold values, above which bulk density becomes limiting for root penetration. Using this review to deduce reference values for the soil texture at our study site (loam), the optimal bulk density is approximately 1.4 g cm^{-3}, while the limiting bulk density ranges between approximately 1.55 and 1.7 g cm^{-3}. The bulk densities data at 30 and 60 cm depth were elevated with median values varying between 1.55 and 1.65 g cm^3 for the loosened and reference soils. In the compacted treatment the bulk density was significantly larger than 1.7 g cm^3, clearly indicating a heavy compaction with restricted root accessibility. The latter is confirmed by the absence of cylindrical POM in the X-ray images of the compacted treatment at 60 cm depth (Fig. 9b). The small bulk density variance for this treatment and depth suggests a relatively homogeneous degree of compaction.

It is known that soil compaction destroys primarily the largest pores in the soil (Keller et al., 2019). Most compacted subsoils exhibited macroporosities ($\varnothing > 30$ µm) below the threshold for air-capacity of 0.05 cm^3 cm^{-3} (Horn and Fleige, 2009). Both, loosened and reference treatment soils exhibited air-capacities of 0.06 cm^3 cm^{-3}, thus slightly above the threshold, indicating a positive effect of the mechanical soil loosening. The water retention data (Fig. 3b–d) and the increased grey-values of the imaged soil matrix (Fig. 6) indicate that the compaction not only diminished the amount of large macropores ($\varnothing >$ app. 100 µm) but also the volume of smaller pores that were not resolved in the X-ray image. In the compacted soil, the volume of large mesopores was reduced, which are important for soil life as they contribute to the plant available water and also are pathways in which water and nutrients are transported when the soil is at field capacity (Moyano et al., 2013). In contrast, the large mesopore ($30 \geq \varnothing > 10$ µm) volume at 30 and 60 cm

depth was largest for the loosened soil. We suppose that pores of this size persisted also 10 months after the soil loosening, when we collected our soil samples, while larger pores were preferentially re-filled or shrunken due to consolidation of the loosened soil.

In contrast to the compacted soil, the samples from the loosened treatment exhibited a larger variance of the bulk density and porosities at 30 and 60 cm depth (Fig. 3) than the reference soil. This reflects an assembly of large compacted clods (diameter ≫ 5 cm) surrounded by loosely packed fraggregates (Fig. 5b) that were created during the soil loosening process with the digger. As the soil sampler used in our study only had a height and a diameter approximately 5 cm, the large variability stems from the fact that we sampled sometimes the inside of the compacted clod and other times the rather loosely packed aggregates. In addition, the spatial variance in bulk density was also largest in the loosened treatment at the micro-scale as it can be seen in the X-ray image histograms (Fig. 6).

4.3. Presence of biopores in the subsoil

It is reasonable to assume that prior to the compaction the abundance of biopores in the subsoil of the compacted and loosened treatments had been similar to the one in the reference soil. It then follows that the compaction event had destroyed the majority of the imaged biopores formerly present under the excavation pile. It is not possible to appraise from our data whether the few detected biopores were relicts that had persisted during compaction or were newly created after the compaction event. The time since the end of compaction (approximately ø) and loosening (approximately 10 months) was, in any case, insufficient to restore a level of biopores similar to the one in the reference soil. The fact that more biopores were found in the loosened treatments indicates that the amelioration measure indeed acted towards a faster recovery of a favourable soil structure (Keller et al., 2021). Fig. 2a illustrates that the original compaction was not homogeneously spread over the investigated area. Instead, prior to the loosening operation, the loosened treatment exhibited larger penetration resistances than the compacted treatment. Therefore, the original biopore destruction can be assumed to have been at least as thorough as in the compacted treatment, if not worst. That there were more biopores identifiable in the loosened than in the compacted treatment underlines the beneficial effects of the soil loosening approach.

4.4. Connectivity of imaged macropore networks

It is commonly stated that a larger Gamma connectivity indicates a better-connected pore network (Jarvis et al., 2017). In our study, however, the compaction led to the reduction of almost all macropores and large mesopores in the subsoil (Fig. 3b–d). The few remaining image-resolvable macropores were relatively large (Fig. 5a). At the same time, small and isolated pore-clusters were almost completely absent in the images of the compacted soil. Both features led to relatively large Gamma connectivities, despite the obviously very poor connectivity of these pore networks. In addition, the smallest Euler numbers, which are generally interpreted as signalling better connected pore networks (Vogel et al., 2010), occurred in the compacted treatment. Again, this was caused by the absence of small isolated pore-clusters and not by the presence of an interconnected pore network.

In contrast to the Gamma connectivity and the Euler number, the measures derived from percolation theory quantified the degraded state of the imaged pore networks in the compacted soil samples more adequately. The fraction of samples with imaged percolating pore networks illustrates that only the reference soil exhibited imaged pore-clusters that connected their top and bottom surfaces (Fig. 8c). It follows, that only the reference soil samples had critical pore diameters in the subsoil that were predominantly larger than the image resolution (Fig. 8d). The indices derived from percolation theory correctly quantify the superior connectivity in the imaged pore networks of the reference soil. The reference soil contained the largest fraction of biopores, which tend to be connected over large distances. The soil loosening, in contrast, could either not restore the soil percolation properties for the large macropores or was too unstable to maintain such connections for the approximately 10 months since the loosening operation.

4.5. Oxygen diffusivity and air permeability

The subsoil aeration properties at −100 hPa in all treatments were almost exclusively below the critical thresholds of 0.01 (oxygen diffusivity) and 8.6 μm (air permeability) reported in Horn and Fleige, (2009). While this is supposed to indicate deficient soil aeration, there are doubts if these threshold values are useful to appraise subsoil aeration (Lebert et al., 2007). Instead, more insight may be gained by comparing the soil aeration properties of the subsoils in our study with measurements from different studies, for example the one published by Keller et al., (2017). These authors investigated the soils of the Soil Structure Observatory (SSO), which is another soil compaction experiment in Switzerland. They evaluated oxygen diffusivities of undisturbed subsoil samples with identical dimensions from identical sampling depths as the ones used in our study. At a matrix potential of −100 hPa, the diffusivities from the SSO compacted treatment were larger than the diffusivities found for the reference soil in our study. This is further evidence hinting that the subsoil of the reference plots in our study did not contain well-developed macropore networks. In any event, in our study, subsoil loosening improved diffusivity and air permeability for the lowest investigated soil depth and for matrix potentials of −300 hPa. Here, the values were largest for the loosened soil. It follows that the soil loosening seemed to improve especially the connectivity of the large mesopores.

If we postulate full wettability of the soil and an effective image resolution of 126 μm, the Young-Laplace law predicts that all connected imaged pores should have drained at a matrix potential of −24 hPa. It follows, that the imaged macropore network is a reasonable approximation to the air-filled macropore system at a matrix potential of −30 hPa. Moreover, it was recently demonstrated that permeability in undisturbed soils is approximately proportional to the square of the critical pore diameter, which is in accordance with predictions from percolation theory, more specifically critical path analysis (Koestel et al., 2018; Schlüter et al., 2020). We therefore expected to observe the largest air permeabilities at −30 hPa in the reference soil, where the critical pore diameters were largest. However, the measured air permeabilities at this matrix potential were all equally small in the subsoils in all treatments. We suspect that water entrapment influenced the air permeability measurements. Alternatively, it may be that pore bottlenecks existed in the top and bottommost parts of the investigated soil samples that could not be evaluated in the X-ray images due to Feldkamp imaging artefacts. Such bottlenecks could have been unintentionally introduced during sample preparation and wetting.

4.6. Potential feedbacks for topsoil structure evolution

As a corollary, we found smaller microporosities and worse pore connectivity in the topsoil of the loosened treatment (Figs. 7 and 8) that also coincided with slightly lower air permeabilities and oxygen diffusions (Fig. 10a and d) and may be related with a lower abundance of biopores in the topsoil of this treatment (Fig. 9). This appears to be a feedback mechanism of the subsoil compaction state on the topsoil that was also apparent in the emergence and establishment of different plant species in the compacted (predominantly alfalfa) and loosened (predominantly rye grass) treatments, albeit both treatments had been sown at the same time and with the same seed mixture. We suggest to investigate the processes of interaction of top and subsoil in future research projects.

5. Conclusion

Our data showed that, in the light of the large penetration resistances, bulk densities, low macroporosities and aeration properties in all the investigated subsoils, root growth may have been restricted in all treatments, even in the reference plots. However, soil loosening significantly alleviated the compaction state of the previously heavily compacted subsoil. Its beneficial effects are reflected in larger macro ($ø > 30$ μm) and mesoporosities ($30 \geq ø > 10$ μm), a less dense imaged soil matrix and better aeration properties than the compacted treatment. Maybe most convincing are the relatively larger abundance of imaged biopores as well as roots and root-like POM after soil loosening. While the physical properties in the subsoil of the reference plots were far from optimal for soil fertility, it still contained a macropore network that was dominated by biopores. In contrast, the loosened plots featured a macropore network consisting almost entirely of cracks and voids between soil fraggregates. While the soil loosening improved the soil structure in the short term, additional monitoring is required to evaluate if the improved soil structure also supports soil recovery in the long-term.

Our study also yielded two main corollary results. Firstly, we found strong evidence that the topsoil functioning was affected by whether the subsoil was compact or loosened. We recommend to investigate the processes behind this and similar observations in future research. Secondly, we became aware that frequently applied pore-network connectivity measures for X-ray image analyses of soil samples, namely the Gamma connectivity and the Euler number, need to be interpreted with care when applied to pore networks in heavily compacted soils. We recommend using measures derived from percolation theory, like the fraction of soil samples with a percolating pore network or the critical pore diameter.

CRediT authorship contribution statement

Alina Widmer: Writing – review & editing, Writing – original draft, Visualization, Investigation, Formal analysis, Data curation. **Alice Johannes:** Writing – review & editing, Project administration, Investigation, Funding acquisition, Conceptualization. **Mario Fontana:** Writing – review & editing, Investigation. **Marlies Sommer:** Validation, Investigation. **Saïd Elfouki:** Investigation. **Luca Bragazza:** Writing – review & editing, Resources, Project administration, Funding acquisition, Conceptualization. **John Koestel:** Writing – review & editing, Writing – original draft, Supervision, Software, Methodology, Investigation, Conceptualization.

Declaration of competing interest

The authors declare that they have no known competing financial interests or personal relationships that could have appeared to influence the work reported in this paper.

Acknowledgement

This research was funded by the “Swiss Federal Office for the Environment” through the project ROCSUB (21.0011.PJ/BAFU-D-48633401/2533), and by Agroscope as part of the “Work Program 2022–2025”.

Data availability

Data will be made available on request.

References

Batey, T., 2009. Soil compaction and soil management - a review. Soil Use Manage. 25 (4), 335–345.
Bengough, A.G., McKenzie, B.M., Hallett, P.D., Valentine, T.A., 2011. Root elongation, water stress, and mechanical impedance: a review of limiting stresses and beneficial root tip traits. J. Exp. Bot. 62 (1), 59–68.
Berisso, F.E., Schjønning, P., Keller, T., Lamandé, M., Etana, A., de Jonge, L.W., Iversen, B.V., Arvidsson, J., Forkman, J., 2012. Persistent effects of subsoil compaction on pore size distribution and gas transport in a loamy soil. Soil Tillage Res. 122, 42–51.
Berli, M., Kulli, B., Attinger, W., Keller, M., Leuenberger, J., Flühler, H., Springman, S.M., Schulin, R., 2004. Compaction of agricultural and forest subsoils by tracked heavy construction machinery. Soil and Tillage Research 75 (1), 37–52.
Bonard, L., 1982. Les sols du domaine de Changins, Etudé regionale. Projektnummer des Kartierdienstes Nr. 128.
Colombi, T., Torres, L.C., Walter, A., Keller, T., 2018. Feedbacks between soil penetration resistance, root architecture and water uptake limit water accessibility and crop growth – a vicious circle. Sci. Total Environ. 626, 1026–1035.
Cresswell, H.P., Kirkegaard, J.A., 1995. Subsoil amelioration by plant-roots - the process and the evidence. Soil Res. 33 (2), 221–239.
Dexter, A.R., 1988. Advances in characterization of soil structure. Soil Tillage Res. 11 (3–4), 199–238.
Drew, M.C., 1992. Soil aeration and plant root metabolism. Soil Sci. 154 (4).
Etana, A., Larsbo, M., Keller, T., Arvidsson, J., Schjønning, P., Forkman, J., Jarvis, N., 2013. Persistent subsoil compaction and its effects on preferential flow patterns in a loamy till soil. Geoderma 192, 430–436.
Gao, W., Hodgkinson, L., Jin, K., Watts, C.W., Ashton, R.W., Shen, J., Ren, T., Dodd, I.C., Binley, A., Phillips, A.L., Hedden, P., Hawkesford, M.J., Whalley, W.R., 2016. Deep roots and soil structure. Plant Cell Environ. 39 (8), 1662–1668.
Garland, G., Koestel, J., Johannes, A., Heller, O., Doetterl, S., Or, D., Keller, T., 2024. Perspectives on the misconception of levitating soil aggregates. Soil 10 (1), 23–31.
Håkansson, I., Reeder, R.C., 1994. Subsoil compaction by vehicles with high axle load—extent, persistence and crop response. Soil Tillage Res. 29 (2), 277–304.
Hamza, M.A., Anderson, W.K., 2005. Soil compaction in cropping systems - a review of the nature, causes and possible solutions. Soil Tillage Res. 82 (2), 121–145.
Horn, R., Fleige, H., 2009. Risk assessment of subsoil compaction for arable soils in Northwest Germany at farm scale. Soil Tillage Res. 102 (2), 201–208.
IUSS, 2022. Working Group WRB. World Reference Base for Soil Resources. International Soil Classification System for Naming Soils and Creating Legends for Soil Maps, fourth ed. International Union of Soil Sciences (IUSS), Vienna, Austria.
Jarvis, N., Larsbo, M., Koestel, J., 2017. Connectivity and percolation of structural pore networks in a cultivated silt loam soil quantified by X-ray tomography. Geoderma 287, 71–79.
Kaufmann, M., Tobias, S., Schulin, R., 2010. Comparison of critical limits for crop plant growth based on different indicators for the state of soil compaction. J. Plant Nutr. Soil Sci. 173 (4), 573–583.
Kautz, T., Amelung, W., Ewert, F., Gaiser, T., Horn, R., Jahn, R., Javaux, M., Kemna, A., Kuzyakov, Y., Munch, J.-C., Pätzold, S., Peth, S., Scherer, H.W., Schloter, M., Schneider, H., Vanderborght, J., Vetterlein, D., Walter, A., Wiesenberg, G.L.B., Köpke, U., 2013. Nutrient acquisition from arable subsoils in temperate climates: a review. Soil Biol. Biochem. 57, 1003–1022.
Keller, T., Colombi, T., Ruiz, S., Manalili, M.P., Rek, J., Stadelmann, V., Wunderli, H., Breitenstein, D., Reiser, R., Oberholzer, H., Schymanski, S., Romero-Ruiz, A., Linde, N., Weisskopf, P., Walter, A., Or, D., 2017. Long-term soil structure observatory for monitoring post-compaction evolution of soil structure. Vadose Zone J. 16 (4).
Keller, T., Colombi, T., Ruiz, S., Schymanski, S.J., Weisskopf, P., Koestel, J., Sommer, M., Stadelmann, V., Breitenstein, D., Kirchgessner, N., Walter, A., Or, D., 2021. Soil structure recovery following compaction: short-term evolution of soil physical properties in a loamy soil. Soil Sci. Soc. Am. J. 85 (4), 1002–1020.
Keller, T., Sandin, M., Colombi, T., Horn, R., Or, D., 2019. Historical increase in agricultural machinery weights enhanced soil stress levels and adversely affected soil functioning. Soil Tillage Res. 194.
Kim, H., Anderson, S.H., Motavalli, P.P., Gantzer, C.J., 2010. Compaction effects on soil macropore geometry and related parameters for an arable field. Geoderma 160 (2), 244–251.
Koestel, J., 2018. SoilJ: an ImageJ plugin for the semiautomatic processing of three-dimensional X-ray images of soils. Vadose Zone J. 17 (1).
Koestel, J., Dathe, A., Skaggs, T.H., Klakegg, O., Ahmad, M.A., Babko, M., Giménez, D., Farkas, C., Nemes, A., Jarvis, N., 2018. Estimating the permeability of naturally structured soil from percolation theory and pore space characteristics imaged by X-ray. Water Resour. Res. 54 (11), 9255–9263.
Kremer, J., Wolf, B., Matthies, D., 2002. Verformungsverhalten künstlicher Makroporen unter variierenden Druck- und Bodenfeuchtebedingungen. J. Plant Nutr. Soil Sci. 165 (5), 627–633.
Kudo, H., Saito, T., 1994. Derivation and implementation of a cone-beam reconstruction algorithm for nonplanar orbits. IEEE Trans. Med. Imaging 13, 196–211.
Lamandé, M., Wildenschild, D., Berisso, F.E., Garbout, A., Marsh, M., Moldrup, P., Keller, T., Hansen, S.B., De Jonge, L.W., Schjønning, P., 2013. X-ray CT and laboratory measurements on glacial till subsoil cores: assessment of inherent and compaction-affected soil structure characteristics. Soil Sci. 178 (7), 359–368.
Lebert, M., Böken, H., Glante, F., 2007. Soil compaction—indicators for the assessment of harmful changes to the soil in the context of the German federal soil protection act. J. Environ. Manage. 82 (3), 388–397.
Legland, D., Arganda-Carreras, I., Andrey, P., 2016. MorphoLibJ: integrated library and plugins for mathematical morphology with ImageJ. Bioinformatics 32 (22), 3532–3534.
Lipiec, J., Hatano, R., 2003. Quantification of compaction effects on soil physical properties and crop growth. Geoderma 116 (1–2), 107–136.

Lucas, M., Schlüter, S., Vogel, H.J., Vetterlein, D., 2019. Soil structure formation along an agricultural chronosequence. Geoderma 350, 61–72.
Martinez, I., Chervet, A., Weisskopf, P., Sturny, W.G., Rek, J., Keller, T., 2016. Two decades of no-till in the Oberacker long-term field experiment: part II. Soil porosity and gas transport parameters. Soil Tillage Res. 163, 130–140.
Meurer, K.H.E., Haddaway, N.R., Bolinder, M.A., Kätterer, T., 2018. Tillage intensity affects total SOC stocks in boreo-temperate regions only in the topsoil—a systematic review using an ESM approach. Earth Sci. Rev. 177, 613–622.
Mossadeghi-Björklund, M., Arvidsson, J., Keller, T., Koestel, J., Lamandé, M., Larsbo, M., Jarvis, N., 2016. Effects of subsoil compaction on hydraulic properties and preferential flow in a Swedish clay soil. Soil Tillage Res. 156, 91–98.
Moyano, F.E., Manzoni, S., Chenu, C., 2013. Responses of soil heterotrophic respiration to moisture availability: an exploration of processes and models. Soil Biol. Biochem. 59, 72–85.
Munkholm, L.J., Schjønning, P., Jørgensen, M.H., Thorup-Kristensen, K., 2005. Mitigation of subsoil recompaction by light traffic and on-land ploughing: II. Root and yield response. Soil Tillage Res. 80 (1), 159–170.
Ollion, J., Cochennec, J., Loll, F., Escudé, C., Boudier, T., 2013. TANGO: a generic tool for high-throughput 3D image analysis for studying nuclear organization. Bioinformatics 29 (14), 1840–1841.
Peng, X., Horn, R., 2008. Time-dependent, anisotropic pore structure and soil strength in a 10-year period after intensive tractor wheeling under conservation and conventional tillage. J. Plant Nutr. Soil Sci. 171 (6), 936–944.
Phalempin, M., Lippold, E., Vetterlein, D., Schlüter, S., 2021. An improved method for the segmentation of roots from X-ray computed tomography 3D images: Rootine vol 2. Plant Methods 17, 39.
Pöhlitz, J., Rücknagel, J., Schlüter, S., Vogel, H.-J., Christen, O., 2019. Computed tomography as an extension of classical methods in the analysis of soil compaction, exemplified on samples from two tillage treatments and at two moisture tensions. Geoderma 346, 52–62.
Pulido-Moncada, M., Katuwal, S., Ren, L., Cornelis, W., Munkholm, L., 2020. Impact of potential bio-subsoilers on pore network of a severely compacted subsoil. Geoderma 363, 114154.
Rabot, E., Wiesmeier, M., Schlüter, S., Vogel, H.J., 2018. Soil structure as an indicator of soil functions: a review. Geoderma 314, 122–137.
Renard, P., Allard, D., 2013. Connectivity metrics for subsurface flow and transport. Adv. Water Resour. 51, 168–196.
Rumpel, C., Chabbi, A., Marschner, B., 2012. Carbon Storage and Sequestration in Subsoil Horizons: Knowledge, Gaps and Potentials. In: Lal, R., Lorenz, K., Hüttl, R.F., Schneider, B.U., von Braun, J. (Eds.), Recarbonization of the Biosphere: Ecosystems and the Global Carbon Cycle. Springer, Netherlands, Dordrecht, pp. 445–464.
Schäffer, B., Attinger, W., Schulin, R., 2007. Compaction of restored soil by heavy agricultural machinery—soil physical and mechanical aspects. Soil Tillage Res. 93 (1), 28–43.
Schäffer, B., Mueller, T.L., Stauber, M., Müller, R., Keller, M., Schulin, R., 2008a. Soil and macro-pores under uniaxial compression. II. Morphometric analysis of macro-pore stability in undisturbed and repacked soil. Geoderma 146 (1), 175–182.
Schäffer, B., Stauber, M., Mueller, T.L., Müller, R., Schulin, R., 2008b. Soil and macro-pores under uniaxial compression. I. Mechanical stability of repacked soil and deformation of different types of macro-pores. Geoderma 146 (1), 183–191.
Schindelin, J., Arganda-Carreras, I., Frise, E., Kaynig, V., Longair, M., Pietzsch, T., Preibisch, S., Rueden, C., Saalfeld, S., Schmid, B., Tinevez, J.-Y., White, D.J., Hartenstein, V., Eliceiri, K., Tomancak, P., Cardona, A., 2012. Fiji: an open-source platform for biological-image analysis. Nat. Methods 9 (7), 676–682.
Schjønning, P., Eden, M., Moldrup, P., de Jonge, L.W., 2013. Two-chamber, two-gas and one-chamber, one-gas methods for measuring the soil-gas diffusion coefficient: validation and Inter-calibration. Soil Sci. Soc. Am. J. 77 (3), 729–740.
Schjønning, P., van den Akker, J.J.H., Keller, T., Greve, M.H., Lamandé, M., Simojoki, A., Stettler, M., Arvidsson, J., Breuning-Madsen, H., 2015. Driver-pressure-state-impact-response (DPSIR) analysis and risk assessment for soil compaction-a European perspective. Adv. Agron. 183–237.
Schlüter, S., Albrecht, L., Schwärzel, K., Kreiselmeier, J., 2020. Long-term effects of conventional tillage and no-tillage on saturated and near-saturated hydraulic conductivity – Can their prediction be improved by pore metrics obtained with X-ray CT? Geoderma 361.
Schneider, F., Don, A., Hennings, I., Schmittmann, O., Seidel, S.J., 2017. The effect of deep tillage on crop yield – what do we really know? Soil Tillage Res. 174, 193–204.
Sinnett, D., Poole, J., Hutchings, T.R., 2006. The efficacy of three techniques to alleviate soil compaction at a restored sand and gravel quarry. Soil Use Manage. 22 (4), 362–371.
Spoor, G., 2006. Alleviation of soil compaction: requirements, equipment and techniques. Soil Use Manage. 22 (2), 113–122.
Tian, M., Whalley, W.R., Zhou, H., Ren, T., Gao, W., 2023. Does no-tillage mitigate the negative effects of harvest compaction on soil pore characteristics in Northeast China? Soil Tillage Res. 233, 105787.
Vaz, C.M.P., Manieri, J.M., de Maria, I.C., Tuller, M., 2011. Modeling and correction of soil penetration resistance for varying soil water content. Geoderma 166 (1), 92–101.
Vogel, H.J., Weller, U., Schlüter, S., 2010. Quantification of soil structure based on Minkowski functions. Comput. Geosci. 36 (10), 1236–1245.